

# Germanium quantum dots prepared by direct annealing of as-deposited amorphous films: Structure and optical properties

Qijiang Shu<sup>a</sup>, Linjing Yang<sup>a</sup>, Xicheng Zhang<sup>a</sup>, Fuhua Yang<sup>a,\*</sup>, Pengru Huang<sup>b,\*</sup>

<sup>a</sup> Institute of Information, Yunnan University of Chinese Medicine, Kunming 650500 China

<sup>b</sup> Guangxi Key Laboratory of Information Materials and Guangxi Collaborative Innovation Center of Structure and Property for New Energy and Materials, School of Material Science & Engineering, Guilin University of Electronic Technology, Guilin 541004 China

\*Corresponding authors, e-mail: yangfuhua@ynucm.edu.cn, pengruhuang@guet.edu.cn

Received 23 Apr 2023, Accepted 17 Mar 2025

Available online 1 May 2025

**ABSTRACT:** We propose a method for annealing amorphous silicon-based germanium (Ge/Si) films to fabricate Ge quantum dots (QDs). To this end, the evolution of the morphology and properties of a Ge-Si composite layer deposited by magnetron sputtering at room temperature followed by annealing at different temperatures is studied with the aid of tests such as atomic force microscopy, scanning electron microscope, X-ray photoelectron spectroscopy, Raman, and photoluminescence PL. The results show that as the annealing temperature increases from 450 °C to 850 °C, enhanced atom migration, improved crystallization, thermal stress from expansion coefficient differences, and high-temperature Ostwald ripening synergistically promote the formation of Ge QDs. The QD size grows continuously, while their density first increases and then decreases. PL peaks of QDs are observed in those samples with high crystallinity, high density, and small size of Ge QDs, in which the sample obtained by annealing at 650 °C exhibits relatively optimal morphological structure and optical properties. The method is expected to be applied to the multiple Ge-Si composite layers stacked at room temperature to produce multilayer Ge/Si QDs, which provides a new idea to solve the problems of low growth efficiency, severe atomic intermixing, and poor homogeneity of QDs in the multilayer structure in the current conventional method, and our results lay a good foundation for this idea.

**KEYWORDS:** Ge/Si, quantum dots, amorphous films, fabrication, thermoelectric materials, optoelectronic properties, photoluminescence

## INTRODUCTION

Quantum dots (QDs), spanning carbon-based QDs, Cd-Se/ZnS core-shell QDs, silicon-based germanium QDs (Ge/Si QDs), etc., have attracted significant attention due to their tunable size, shape, and composition, enabling their versatile applications in biomedicine, photonics, optoelectronics, and thermoelectrics [1–3]. The fabrication of Ge/Si QDs with tunable size and positional arrangement has been the subject of extensive research since the 1990s [4, 5]. Several approaches have been proposed for the formation of Ge/Si QDs, including chemical synthesis [6], epitaxial growth [7], lithographic patterning [8], and electrostatic-gate definition based on two-dimensional electron-gas heterostructures [9]. Many exotic electronic and optical properties of Ge/Si QDs have been progressively applied to high-performance semiconductor devices such as QD registers [10], QD detectors [11], QD memories [12], QD solar cells [13], and QD-based thermoelectric devices [14].

The key to implementing QD devices for practical applications lies in having an unprecedentedly high degree of control over the crystallinity, size, shape, density or number, and spatial location of QDs, all of which are essentially important for optimizing device

performance. This has inspired continuous innovation and development in methods for preparing QDs, leading to numerous breakthroughs in recent years. For example, Grydlik et al [15] use molecular beam epitaxy (MBE) combining with *in situ* low-energy Ge ion bombardment to embed Ge QDs into defect-free crystalline silicon matrices; these QDs exhibit remarkable optical properties of dramatically shortened carrier lifetimes and negligible thermal quenching of the photoluminescence up to room temperature. Huang et al [16] report the novel tunability of the diameters and spacings of paired Ge double QDs using nano-spacer technology in combination with selective oxidation of  $\text{Si}_{0.85}\text{Ge}_{0.15}$  at high temperatures. They show the strategy to achieve high symmetry within the Ge double QDs in terms of the individual QD diameters as well as the coupling barriers between the QDs and external electrodes in close proximity. Chu et al [17] introduce their work of using low growth temperature (Ge below 400 °C, Si below 500 °C) to inhibit the formation of Ge nanoislands in multilayer Ge/Si films grown by low-pressure chemical vapor deposition (CVD) to fabricate and demonstrate stacked Ge nanosheets GAA FET CMOS inverter. Smagina et al [18] find that with a certain choice of pit-patterned substrate parameters (diameter of pits and their spatial period), the ordered

Ge/Si QDs epitaxial on the pit-patterned “silicon-on-insulator” show multiple narrow peaks of photoluminescence, and the luminescence enhancement effect persists up to room temperature. Peng et al [19] develop Ge QDs and Sn precipitation SiGeSn hybrid film through ultrafast high-temperature annealing of a P-ion implanted SiGeSn film on a Si/SiO<sub>2</sub> substrate, offering a novel perspective for high-performance thermoelectric materials.

Based on the existing research results, 2 highlighted issues have gradually become the focus. First, considering most of the manufacturing technologies (MBE, CVD, solid phase epitaxy, etc.) for QDs, high requirements for temperature control (MBE), reaction products that may become surface impurities (CVD), and especially their inherent problems such as expensive equipment, high operating costs, and low growth rates have become the main obstacles to the industrial production of high-quality and usable QDs.

Second, the growth of multilayer QDs is basically done by a top-down or bottom-up layer-by-layer stacking method [20], as illustrated in Fig. 1(a). Since such processes are carried out at high temperatures that guarantee the crystallization of the films, those QDs grown earlier have to undergo longer-time annealing, which often leads to a typical Ostwald ripening or to a significant interatomic diffusion between them and the upper and lower layers [21, 22], and these changes produce a stress modulation on the deposited layers above them which affects the QD growth, resulting in significant differences between the QDs of different layers and then a decrease or even disappearance of the desired optoelectronic properties.

Magnetron sputtering is expected to be a new way to solve the first problem, offering a deposition rate hundreds of times higher and lower equipment operating costs compared to conventional techniques such as MBE and CVD. These advantages have attracted considerable research attention over the past decade [22–26], which include the preparation of QDs under different conditions of sputtering power, working gas, deposition thickness, growth temperature, annealing, etc. Although the complete evolution mechanism and mature structure optimization schemes of the reported QDs still need to be further explored, the obtained results have confirmed the feasibility of using magnetron sputtering to grow Ge/Si QDs at high speed. In this context, a novel approach that promises to solve both of the above problems simultaneously is proposed. As shown in Fig. 1(b), this approach is carried out in 2 steps, and the first step is the deposition of multilayer films by magnetron sputtering, which are grown at high speed at room temperature to ensure that no significant atomic interdiffusion occurs between the layers. The second step is *in situ* annealing of these deposited films to drive the simultaneous formation of Ge QDs in each Ge layer to ensure the homogeneity

of these dots. The great challenge faced by this method is that the structural evolution of Ge films is completely different from the traditional mechanism of the Stranski-Krastanow (SK) growth mode that has been understood. Whether such a process can fabricate QDs, the evolution mechanism of these QDs and their appropriate growth parameters need to be explored step by step. The work in this paper focuses on the morphology and photoelectric properties of the Ge surface with a single periodic structure (a Ge-Si composite layer deposited at room temperature) at different annealing temperatures. The results obtained can verify the feasibility of direct annealing of amorphous films to fabricate QDs, which provides not only a new idea for efficient and low-cost fabrication of single-layer QDs but also the necessary empirical parameters and growth mechanisms of QDs with multiple periodic structures (multiple Ge-Si composite layers) using this method. That is, this work is an important and necessary first step to gradually realize the vision in Fig. 1(b).

## MATERIALS AND METHODS

All samples are grown in a magnetron sputtering system (FJL560III type, Sky Technology Development Co., Ltd., Chinese Academy of Sciences, Shenyang, China) under a background pressure of  $1.0 \times 10^{-5}$  Pa. The experiment utilizes single-side polished (100) Si wafers with a thickness of 500  $\mu\text{m}$  (LONGi Green Energy Technology Co., Ltd., Xi'an, China) as the substrates. At room temperature, a 50 nm Si film followed by a 25 nm Ge film are sequentially sputtered onto the substrate surface. Subsequently, the integrated temperature controller within the sputtering system is used to rapidly heat the deposited bilayer films to the predetermined annealing temperature, maintaining a constant temperature for 10 min to complete *in situ* annealing. For comparison, temperatures of 25, 450, 550, 650, 750, and 850 °C are selected as annealing temperatures, and the samples are then designated as 25, 450, 550, 650, 750, and 850. After annealing, the samples are naturally cooled to room temperature and then transferred into nitrogen-filled sample bags for further analysis. Atomic force microscopy (AFM; SPA-400SPM, SEIKO Co., Ltd., Tokyo, Japan) and scanning electron microscope (SEM; FEI Quanta 200, FEI Company, Hillsboro, US) are used to characterize the surface morphology of the samples, X-ray photoelectron spectroscopy (XPS; Thermo Scientific K-Alpha, Thermo Fisher Scientific Inc., Waltham, US) is used to test the elemental composition and structural changes of the sample surface, and Raman (Renishaw inVia, Renishaw plc, Wotton-under-Edge, UK) and photoluminescence (PL; Gemini-180, Horiba Scientific, Edison, US) tests are used to analyze the crystallographic and optical properties of the QDs on the sample surface.

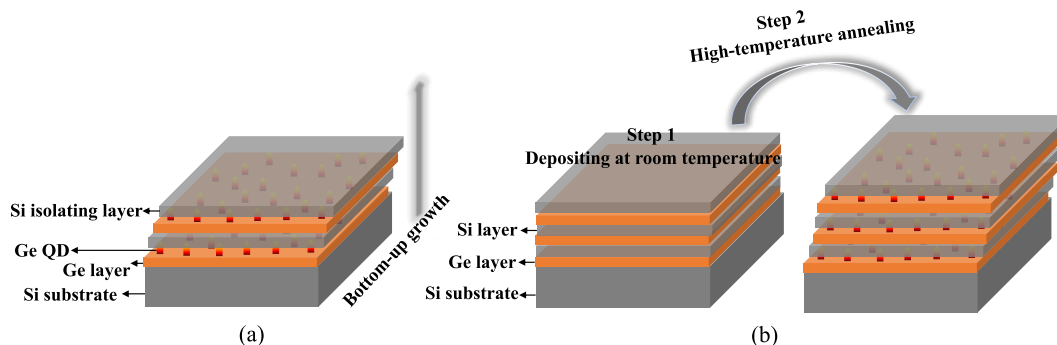


**Fig. 1** Schematic diagram of the growth method of multilayer QDs. (a) The conventional bottom-up self-organized growth process and (b) the proposed idea of employing annealing to drive the film to form QDs directly.

In the above experiments, the Si substrates are cleaned by the Shiraki method and then soaked in 25% HF (Yuntianhua Co., Ltd., Kunming, China) for 60 s to remove the surface oxides and passivate the surface H. The parameters involved in sputtering Si films include RF sputtering mode, sputtering power of 45 W, sputtering pressure of 0.2 Pa, and argon flow rate of 5 sccm, and the corresponding parameters for Ge films are DC sputtering, 35 W, 0.15 Pa, and 10 sccm, respectively. The working gas is argon with a purity of 99.999% (Yigas Co., Ltd., Guangzhou, China), and the target purity of both Si and Ge (Beijing Ryubon New Material Technology Ltd., Beijing, China) is 99.99%. The AFM, SEM, XPS, and Raman measurements are performed at room temperature, while the PL tests are conducted at a low temperature of 7 K, achieved using a liquid helium cooling system. The model of the probe used for AFM measurements is SSS-SEIHR (Nanosensors GmbH, Munich, Germany), the excitation source of XPS is Al-K $\alpha$  x-Ray ( $h\nu = 1486.6$  eV), the excitation source of Raman is an Ar<sup>+</sup> laser with a wavelength of 514.5 nm, and the wavelength and power of the laser used for PL test are 488 nm and 0.8 mW, respectively.

## RESULTS AND DISCUSSION

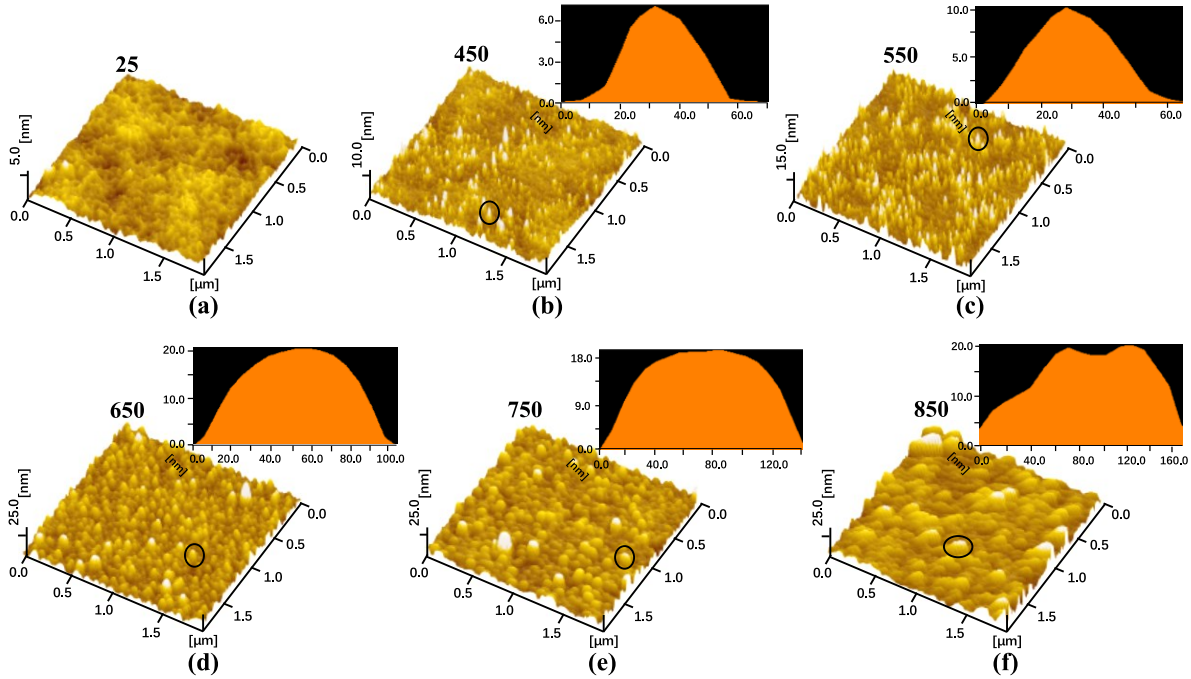
### Morphology evolution of QDs

Fig. 2 shows the surface morphology of the as-deposited Ge films after annealing at different temperatures. They are all obtained using an AFM under the same test conditions. A typical Ge QD on the surface of each sample is marked with a black circle, and the profile and dimensions of this QD are attached as an illustration in the upper right corner of this sample. The results in the figure indicate that for the deposited 25 nm Ge film, the room temperature (sample 25) cannot cause its surface to form Ge QD structures, while the annealing temperature of 450 °C allows the formation of Ge nanoislands with a relatively small density and size on the film surface. With the annealing temperature gradually increasing from 450 °C to 850 °C, these Ge islands gradually evolve from small

ones (~40 nm wide and ~6 nm high) to super large ones (~170 nm wide and ~20 nm high).

Based on AFM measurements, Fig. 3 quantitatively illustrates the changes in the average size (both height and base diameter) and surface density of Ge QDs across various samples as the annealing temperature is gradually increased. In contrast to the continuous increase in the size of the Ge QDs, the density of these dots exhibits a trend of first rising and then decreasing. The temperature of 650 °C represents a significant turning point. Supporting evidence for this assertion includes not only the peak in QD density at 650 °C but also the nearly two-fold maximum increase in QD size from 550 °C to 650 °C (see Fig. 2(c,d)). Furthermore, as shown in Fig. 2, the shape of the QDs predominantly exhibits a pyramidal form at 450 and 550 °C, while transitioning to a dome-shaped form after 650 °C.

According to existing reports, the formation of the self-assembled Ge/Si QDs is mainly driven by the lattice mismatch (~4.2%) between Ge and Si. The evolution of the surface morphology of the deposited Ge film shifts from two-dimensional to three-dimensional (nanoislands) after the deposition thickness slightly exceeds the corresponding wetting-layer thickness (generally several nanometers), i.e., the typical SK growth mode [4]. The films of the samples in this report are all grown at room temperature, their structures are predominantly amorphous, and the Ge thickness is as high as 25 nm, implying that the Ge QDs on the sample surface do not arise in the SK mode, but a more complex result of the comprehensive thermodynamic and kinetic effects. Fig. 4 can give an illustration of the growth mechanism of the QDs on these samples. Fig. 4(a) illustrates the Ge-Si film deposited at room temperature, which has a relatively flat surface with no island structure seen, which is typical of amorphous film subjected to two-dimensional growth, corresponding to sample 25 in Fig. 2(a). When different temperatures are used to anneal the deposited film, on the one hand, some Ge atoms in the amorphous film escape



**Fig. 2** AFM photographs of the surface of Ge films annealed at different temperatures (25, 450, 550, 650, 750, and 850 °C) with 25-nm-thick films and 10-min annealing time. The cross-sectional profiles and corresponding dimensions of typical QDs as indicated by the black circles in each sample are shown in the upper right corner of the photos.

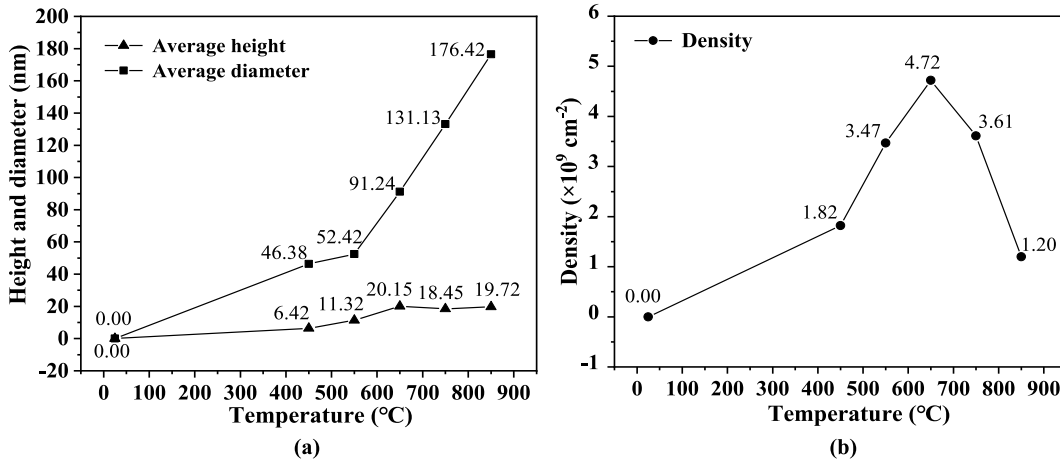


**Fig. 3** Statistics of QD size (average height and average diameter) and QD areal density for each sample annealed at 25, 450, 550, 650, 750, and 850 °C, respectively. (a) corresponding to the QD size and (b) showing the QD density.

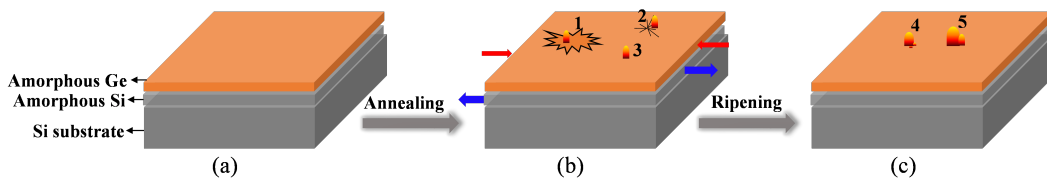


**Fig. 4** Schematic diagram of Ge QDs formed on the surfaces of samples 25, 450, 550, 650, 750, and 850. The colored arrows in the image indicate the direction of the stress on films, 1 the crystalline region, 2 the low chemical potential area caused by stress, 3 nanoislands formed by migration of surface atoms, 4 nanoislands that have grown larger due to the gathering of the surrounding atoms, and 5 super large islands formed by annexing surrounding islands.

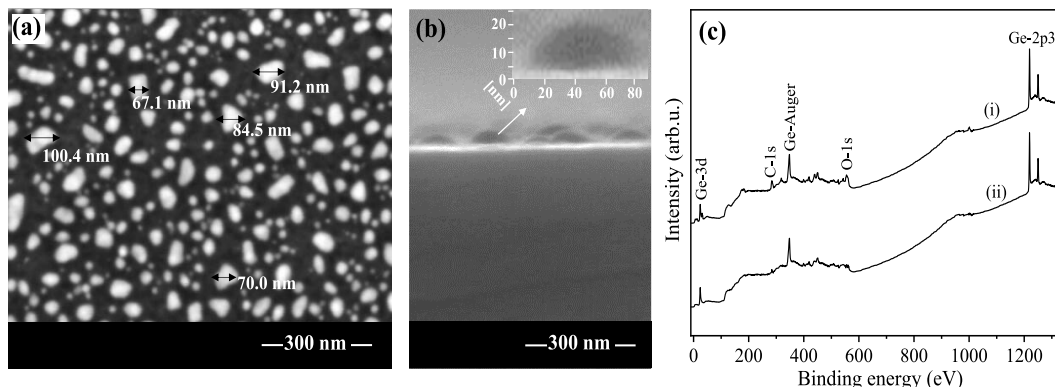


**Fig. 5** The SEM micrographs and the XPS spectra of sample 650. (a) The overhead view and (b) the sectional view of QDs on the sample surface measured by SEM at a magnification of 200000. The size of some typical QDs in (a) and (b) are marked. (c) The recorded XPS spectra of the sample that is sputtered for (i) 0 min and (ii) 10 min, respectively.

from the original surrounding atoms and migrate to the location of the lattice defects, repairing the lattice and crystallizing the local region of the film. The elevated annealing temperature injects more energy into the film system to increase the crystalline regions, thus creating more strain between the crystalline Ge and Si films due to lattice mismatch. The strain energies are released in the form of nanoislands formed on the film surface to maintain the minimum free energy of the system, as illustrated in Fig. 4(b) at 1. On the other hand, during the *in situ* heating to the set annealing temperature, the Si and Ge films will be stressed in different directions due to the difference in thermal expansion coefficients between them ( $\text{Si} < \text{Ge}$ ) [27], as shown by the colored arrows in Fig. 4(b). The transverse compressive stress on the Ge film tends to produce many tiny undulations (stress mutation zones) on its surface as illustrated in Fig. 4(b) at 2. They can be considered the initial forms of Ge QDs, and these initial states are easy to attract surface-migrating Ge atoms to develop into Ge nanoislands of various sizes due to their low chemical potentials during isothermal annealing. Besides that, the high temperature can effectively improve the migration ability of Ge atoms on the film surface, which enhances the probability of the active atoms to meet and coalesce into nuclei and further grow into QDs, and such QDs are illustrated by 3 in Fig. 4(b). It is easy to speculate that both the density and size of the above QDs become larger at a higher annealing temperature (i.e., more crystalline regions, higher film stresses, and stronger atomic mobility), which coincides with the pattern of variation shown for samples 450, 550, and 650 in Fig. 2.

In addition, the increase in the density of QDs implies a decrease in their spacing. When the elastic spaces between QDs overlap each other, these QDs compete to absorb the common atoms around them. Those QDs with low chemical potential can preferen-

tially attract neighboring atoms and expand their own size, as illustrated by 4 in Fig. 4(c). Some large islands that continue to grow in size gradually overlap with the surrounding islands and annex them to develop into super large islands, as shown in Fig. 4(c) at 5. As a result, the density of the islands decreases while the distribution of island sizes becomes broader, which is consistent with the observations for samples annealed at 750 and 850 °C as shown in Fig. 2. This is a typical Ostwald ripening process [28]. Obviously, it is difficult to form QDs with high enough density and surface migrating atoms with high enough energy at too low a temperature to meet the conditions required for ripening, which is the reason why the series of samples in this report exhibits the mechanism process illustrated in Fig. 4(c) only after 650 °C. The excessive temperature causes the phenomenon of large islands annexing small ones (demonstrated by the profile morphology of the typical QD in Fig. 2(f)) to become common, and when these super large islands interconnect in the process of continuous size development, their surface contours evolve into the surface undulations of a two-dimensional film, thereby significantly reducing the island density, as depicted in Fig. 3(b). Additionally, the increase in annealing temperature allows the QD shape to evolve gradually from pyramidal to dome-shaped, which is similar to that reported by Ribeiro et al [29] and Ross et al [30] and is attributed to the result of competition and equilibrium between the surface energy and stress relaxation energy of the samples at different temperatures.

Fig. 5 presents the SEM and XPS measurements of sample 650. Panel (a) shows a top view of the surface QDs of the sample with the lateral dimensions (diameters) of some typical QDs indicated in the figure. Panel (b) displays a side view of the surface QDs with the typical width and height of the QDs also marked in the inset in the upper right corner. Comparing these results with Fig. 2(d), the typical sizes as well as the

**Table 1** The FWHM of Raman peaks of samples 25, 450, 550, 650, 750, and 850.

Sample	FWHM of the Ge-Ge peak (cm <sup>-1</sup> )	FWHM of the Ge-Si peak (cm <sup>-1</sup> )	FWHM of the Si-Si peak (cm <sup>-1</sup> )
25	51.07	—	7.16
450	42.95	—	5.57
550	21.33	—	5.53
650	9.76	—	5.40
750	23.79	32.01	5.25
850	18.47	22.42	5.29

morphological profiles of the QDs displayed are very consistent. It is easy to conclude that the operational mode and probe used for the AFM measurements are suitable and that they suppress the tip convolution effect well enough to make the measurements with the expected accuracy, which is corroborated by an additional measurement method (SEM). (c) is the XPS spectra of the sample, where (i) shows the results measured on the sample surface without sputter etching, and (ii) shows the results measured after the surface has been sputtered for 10 min. As shown in the figure, weak characteristic peaks of C-1s and O-1s are observed in (i), and they almost disappear after sputtering treatment on the sample surface (see (ii)). This result indicates that despite keeping the samples in high-purity nitrogen during transfer, minor contamination and oxidation remain difficult to avoid completely. The presence of clear Ge peaks and the absence of Ge oxide peaks in the spectra indicate that the growth of QDs in a high vacuum environment is unaffected by residual gases, and their impact on QD morphology can be ignored.

### Crystalline structure of QDs

Fig. 6 shows the Raman measurements of all samples with (a) displaying the spectra within the 150 cm<sup>-1</sup>–600 cm<sup>-1</sup> wavenumber range of each sample. Some typical characteristic peaks and their central peak positions are labeled in the figure. (b) and (c) respectively show the Gaussian fitting results of the Ge-Ge and Si-Si peaks of sample 450. Table 1 lists the FWHM (full width at half maximum) values of the characteristic peaks for each sample in Fig. 6(a). As shown in Fig. 6(a), all samples show obvious characteristic peaks of Si-Si bonds, and the corresponding peak positions are relatively close to the peak position of the intrinsic peak of bulk Si at 521 cm<sup>-1</sup>. The statistical values in Table 1 show the variation pattern of the FWHM of these Si-Si peaks gradually decreasing with increasing temperature. Comparison of the FWHM and intensity of each Si-Si peak indicates that the crystallinity of the as-deposited Si film improves with increasing annealing temperature. In fact, Si films that have undergone low-temperature annealing (such as 25, 450, and 550 °C) contain non-negligible

amorphous Si, which can be seen from the multi-peak fitting results of sample 450 in Fig. 6(c). The presence of amorphous Si is due to the low annealing temperature, which does not provide sufficient energy for Si atoms to form crystalline nuclei, significantly affecting the Si-Si peak, which is why the Si-Si peak of sample 25 in Fig. 6(a) deviates relatively more from the intrinsic peak and the peak intensity is relatively weak. Furthermore, low annealing temperatures (such as 25, 450, 550, and 650 °C) cannot supply enough energy for atoms to cross the interlayer barrier of Si/Ge contact layer and cause atomic mixing, which can be demonstrated by the absence of characteristic peaks of Ge-Si bonds in Raman spectra. When the annealing temperature is raised to 750 °C, a significant Ge-Si peak is observed, and 850 °C drives the FWHM of the Ge-Si peak to become smaller and the peak position to shift from 398.2 cm<sup>-1</sup> to 402.3 cm<sup>-1</sup>, which can be thought to be mainly caused by the high temperature intensifying the interdiffusion between Ge and Si atoms. Meanwhile, the mixing of atoms at the Ge/Si contact layer induces a large adjustment of the lattice strain, which to some extent adds dislocation defects to the film and also leads to a large fluctuation in the distribution of the chemical potential of the Ge film, which has an important modulating (accelerating) effect on the ripening of the surface Ge nanoislands.

The characteristic peaks of Ge-Ge bonds are observed in all samples, and interestingly, these peaks show significant differences in peak shape and peak position. According to existing literature reports [20, 25, 31], in addition to the influence of changes in crystallinity on peak positions, quantum confinement effects, dislocation defects, atomic mixing, and tensile strain can all drive the Ge-Ge peak away from its intrinsic peak position at 300.5 cm<sup>-1</sup> in the low wavenumber direction (red shift), while compressive strain causes the peak position to deviate from its intrinsic peak in the high wavenumber direction (blue shift). As shown in Fig. 6 and Table 1, the peak position of 267.6 cm<sup>-1</sup> and the FWHM of 51.07 cm<sup>-1</sup> for sample 25 indicate that the Ge film is mainly in an amorphous state. As the annealing temperature increases to 450 °C, the FWHM of the Ge-Ge peak in sample 450 decreases, and the peak shifts to 298.0 cm<sup>-1</sup>. Combined with Fig. 6(b), it can be concluded that the grown Ge film is a mixture of crystalline and amorphous phases. When the annealing temperature is 550 °C, the Ge-Ge peak shape exhibits a better symmetry with a decreased FWHM, and the peak shifts to 300.5 cm<sup>-1</sup>. These behaviors indicate that the Ge in the film has mostly crystallized. That is, the increase in the crystallization rate under annealing temperature regulation is the main reason driving the change in the Ge-Ge peaks of samples 25, 450, and 550. The lower FWHM and higher symmetry of the Raman peak of sample 650 compared to 550 suggest a higher crystallinity of its Ge. Combined

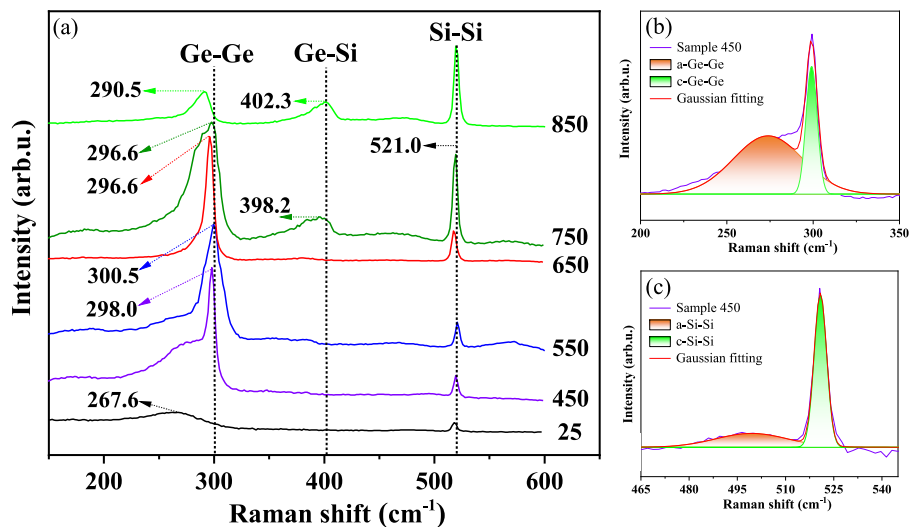


**Fig. 6** The Raman spectra of (a) the QD samples 25, 450, 550, 650, 750, and 850, and the multi-peaks Gaussian fitting of the (b) Ge-Ge and (c) Si-Si signals of sample 450.

with the fact that high-density crystalline QDs are formed on the sample surface, it can be considered that quantum confinement effects drive a  $3.9 \text{ cm}^{-1}$  of redshift ( $300.5 - 296.6 = 3.9$ ) in its Ge-Ge peak position. However, the crystallization rate of Ge does not monotonically increase with the annealing temperature. When the annealing temperature rises from  $650^\circ\text{C}$  to  $850^\circ\text{C}$ , the FWHM of Ge-Ge peaks in samples 750 and 850 increases, and the crystallinity actually deteriorates. The main reason for this phenomenon is the excessive activation energy given to the internal and surface atoms of the Ge film by the excessively high temperature. These atoms cannot stay in the position with low free energy but have some kinetic energy to break free and continue moving. Some atoms even get free from the surface of the Ge islands to move during the ripening process of the nanoislands. These behaviors hinder the regular arrangement (crystallization) of the atoms and even lead to localized cracks and dislocation defects in many crystal regions, resulting in a decrease in the crystallinity of the sample. At the same time, as described in the previous discussion of the Ge-Si peaks, atomic mixing at high temperatures not only leads to lattice relaxation but also promotes merging (ripening) between nanoislands, which are typical kinetic processes for the generation of dislocation defects. Therefore, the red shift in the Ge-Ge peaks of samples 750 and 850 is actually caused by a combination of changes in the Ge crystallization rate, atomic intermixing, and dislocation defects, while quantum confinement effects can be ignored because the size of their nanoislands is too large and the density is too small. Obviously, these inferences obtained from the Raman tests are mutually consistent with the morphological analysis of Ge QDs based on the AFM

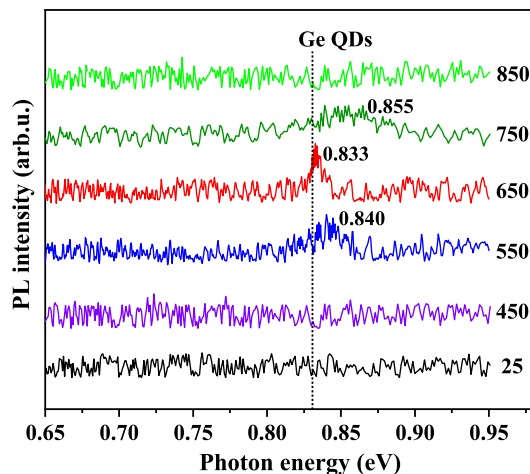


**Fig. 7** PL spectra of samples 25, 450, 550, 650, 750, and 850, recorded at 7 K. The text label in the figure indicates the signals related to the luminescence originated from the recombination of excitons in Ge QDs. The central positions of these PL peaks are marked.

measurements above (Fig. 2 and Fig. 4).

### Optical properties of QDs

To explore the relationship between the morphological structure and the optical properties of the samples, the photoluminescence performance of these prepared samples is tested and shown in Fig. 7. According to the available literature [32, 33], clear observation of the PL peaks of Ge QDs (located near 0.83 eV) often requires the preparation of samples containing multiple layers of Ge QDs with high density and small size because

single-layer QDs tend to have difficulty in capturing enough excitation photons and their corresponding very weak luminescence information is easily drowned in the noise from the underlying film. As shown in Fig. 7, no luminescence peaks of QDs are observed in sample 25, and such a result is consistent with the fact that there are almost no nanoisland structures on the surface of this sample. Although some small-sized nanoislands are formed on the surface of sample 450, their density is too low (see AFM tests), and many are in amorphous or mixed crystal states (see Raman tests), which prevent them from exerting size effects to produce a sufficient number of splitting energy levels, and the excitation light mostly passes through the surface QDs without providing them with enough effective photons, so no luminescence peaks of QDs are observed in this sample. The islands of sample 850 are all super large ones with low density, and their overall morphology is close to the structure of a two-dimensional film with large surface fluctuations. In theory, such islands with a transverse size of nearly 200 nm are difficult to generate the classical splitting energy levels of QDs, so the phenomenon of PL peak absence also occurs in this sample.

Encouragingly, weak PL peaks are observed in samples 550, 650, and 750. Considering the morphological differences between these samples and those without observed emission peaks as well as the positions of these emission peaks [32, 33], it is likely that these peaks originate from QDs on the surface of the samples. The peak of sample 650 shows the smallest FWHM and the strongest intensity, which is attributed to the fact that the surface QDs of sample 650 have the best crystallinity and the highest density (implying the presence of the maximum number of size-dependent splitting levels, which significantly increases the probability of effective coupling with the excitation photons). In the basic model of the quantum confinement effect [34], there is a clear dependence between the energy gap of QD materials and the size of QDs. Specifically, the smaller the size of QDs, the larger the energy gap, which is manifested by the shift of the luminescence peak towards higher photon energy. As shown in Fig. 7, with sample 650 as a reference, the central peak of sample 550 with smaller QDs shifts from 0.833 eV to 0.840 eV, which is most likely caused by the quantum confinement effect, while the relatively weaker peak intensity may be attributed to the lower density of surface QDs. However, contrary to the theoretical model of the quantum confinement effect, the luminescence peak of sample 750 containing QDs with a larger average size is instead shifted in the direction of higher photon energy. This phenomenon is likely caused by an experimental inference discussed in Fig. 6, namely, the presence of large lattice strain adjustments and many dislocation defects in sample 750, which effectively increases the strain relaxation rate of

the material, and the strain relaxation raises the effective energy gap of the material, the luminescence peak position is thus shifted to higher photon energy, and this change dominates the competition with quantum confinement effects. And the relatively weakest peak intensity exhibited by sample 750 coincides with the morphological structure of its QDs having the relatively largest size and smallest density. These results not only confirm that QDs with good morphology and structure (high crystallinity, high density, and small size) do indeed have relatively excellent optical performance but also demonstrate the feasibility of using the direct annealing method to grow QDs. It can be predicted that sample 650 will exhibit relatively optimal optoelectronic performance in optoelectronic devices, and its growth parameters can be used as a basis for further refinements such as changing the Ge deposition thickness, annealing temperature, annealing time, and other factors to create better QDs, which guides the next research work.

It is worth noting that, compared to the single-layer QDs grown via the self-assembled bottom-up SK growth mode reported in conventional studies [35–37] (which have densities of approximately  $10^{10}$ – $10^{11}$   $\text{cm}^{-2}$ , diameters of about 7–30 nm, and heights of approximately 2–6 nm), the QDs obtained in this study exhibit lower density, larger size, and relatively weaker photoluminescence. However, our study introduces a new preparation method that successfully fabricates QDs through direct annealing of as-deposited amorphous films. This approach suggests that future research could enable simultaneous annealing of multilayer films deposited at room temperature, potentially facilitating the formation of multilayer QDs. This provides a new perspective for addressing the inherent issues in traditional bottom-up growth methods for multilayer QDs, where earlier-grown layers face severe maturation and atomic mixing challenges. Although our current work only reports on single-layer QDs, the results establish the feasibility of using this method for multilayer growth and provide a crucial theoretical foundation. Additionally, the method demonstrated, based on magnetron sputtering technology, offers high deposition rates and low operational costs, enhancing the significance of QD preparation. This efficient and cost-effective approach paves a potential pathway for the industrial production of QDs.

## CONCLUSION

In summary, we annealed bilayer films containing 50 nm Ge and 50 nm Si, deposited by magnetron sputtering at 25 °C and at temperatures ranging from 450 °C to 850 °C in 100 °C increments to prepare Si-based Ge QDs with varying morphologies. AFM results indicate that as the annealing temperature increases, the size of Ge QDs grows, transitioning from pyramidal to dome-shaped structures and forming super islands

after 650 °C. The QD density peaks at 650 °C, following a trend of increasing first and then decreasing. These morphological changes are attributed to atomic migration, crystallization, thermal strain, and Ostwald ripening. Raman measurements reveal that the crystallization rate of the Si substrate increases with temperature, while the Ge layer reaches its maximum crystallinity at 650 °C before decreasing due to high-temperature atomic disorder. Shifts in Ge-Ge Raman peaks reflect changes in crystallinity, quantum confinement effects, Ge-Si mixing, and dislocation defects. PL measurements show luminescence peaks at 550, 650, and 750 °C, with 650 °C yielding optimal luminescence due to favorable QD density, size, and lattice relaxation. This study establishes an efficient method for QD preparation, elucidates the morphological and luminescence evolution mechanisms, and offers theoretical and practical insights for overcoming challenges in QD growth, especially in multilayer stacking.

**Acknowledgements:** This work was financially supported by the Basic Research Project of Yunnan Province (No. 202001AU070112), the National Key Research and Development Program (No. 2021YFB3802400), the National Natural Science Foundation of China (No. 52161037), the IUR Innovation Fund of Science and Technology Development Center of the Ministry of Education of China (No. 2021BCA02006), and the TCM Joint Project of Yunnan Province (No. 202301AZ070001-033).

## REFERENCES

1. Yuan H, Yang H, Yuan P, Wang T, Zhou Q (2023) Carbon quantum dots as drug carriers for tumor-associated macrophage repolarization following photothermal therapy. *ScienceAsia* **49**, 627–634.
2. Yin J, Zhang J, Chen M, Yin H, Tian J (2022) Reduction of Cd<sup>2+</sup>/Ag<sup>+</sup>-induced toxicity by 3-mercaptopropionic acid-CdSe/ZnS quantum dots and glutathione-CdSe/ZnS quantum dots in human liver cancer cells. *ScienceAsia* **48**, 414–422.
3. Aouassa M, Bouabdellaoui M, Pessoa WB, Berbezier L, Kallel T, Ettaghzouti T, Yahyaoui M, Saron KM, et al (2024) Growth of Ge QDs-decorated SiGe nanocrystals: Toward integration of quantum dots and Mie resonators in ultrathin film for photodetection and energy harvesting. *ACS Appl Electron Mater* **6**, 3290–3296.
4. Eaglesham DJ, Cerullo M (1990) Dislocation-free Stranski-Krastanow growth of Ge on Si (100). *Phys Rev Lett* **64**, 1943–1946.
5. Hong PY, Lin CH, Wang IH, Chiu YJ, Lee BJ, Kao JC, Huang CH, Lin HC, et al (2023) The amazing world of self-organized Ge quantum dots for Si photonics on SiN platforms. *Appl Phys A* **129**, 126.
6. Karatutlu A, Song M, Wheeler AP, Ersoy O, Little WR, Zhang Y, Puech P, Boi FS, et al (2015) Synthesis and structure of free-standing germanium quantum dots and their application in live cell imaging. *RSC Adv* **5**, 20566–20573.
7. Brehm M, Grydlik M (2017) Site-controlled and advanced epitaxial Ge/Si quantum dots: fabrication, properties, and applications. *Nanotechnology* **28**, 392001.
8. Smagina ZV, Zinovyev VA, Rudin SA, Novikov PL, Rodyakina EE, Dvurechenskii AV (2018) Nucleation sites of Ge nanoislands grown on pit-patterned Si substrate prepared by electron-beam lithography. *J Appl Phys* **123**, 165302.
9. Lawrie W, Eenink H, Hendrickx N, Boter J, Petit L, Amitonov S, Lodari M, Wuetz B, et al (2020) Quantum dot arrays in silicon and germanium. *Appl Phys Lett* **116**, 080501.
10. Wang IH, Hong PY, Peng KP, Lin HC, George T, Li PW (2021) Germanium quantum-dot array with self-aligned electrodes for quantum electronic devices. *Nanomaterials* **11**, 2743–2757.
11. Yakimov AI, Kirienko VV, Bloskhin AA, Utkin DE, Dvurechenskii AV (2021) Near-infrared photoresponse in Ge/Si quantum dots enhanced by photon-trapping hole arrays. *Nanomaterials* **11**, 2302–2310.
12. Kim DW, Kim T, Banerjee SK (2003) Memory characterization of SiGe quantum dot flash memories with HfO<sub>2</sub> and SiO<sub>2</sub> tunneling dielectrics. *IEEE T Electron Dev* **50**, 1823–1829.
13. Parravicini J, Trapani FD, Nelson MD, Rex ZT, Beiter RD, Catelani T, Acciarri MF, Podesta A, et al (2020) Quantum confinement in the spectral response of n-doped germanium quantum dots embedded in an amorphous Si layer for quantum dot-based solar cells. *ACS Appl Nano Mater* **3**, 2813–2821.
14. Pernot N, Stoffel M, Savic I, Pezzoli F, Chen P, Savelli G, Jacquot A, Schumann J, et al (2010) Precise control of thermal conductivity at the nanoscale through individual phonon-scattering barriers. *Nature Mater* **9**, 491–495.
15. Grydlik M, Hackl F, Groiss H, Glaser M, Halilovic A, Fromherz T, Jantsch W, Schäffler F, et al (2016) Lasing from glassy Ge quantum dots in crystalline Si. *ACS Photonics* **3**, 298–303.
16. Huang TL, Peng KP, Chen CL, Lin HC, George T, Li PW (2019) Tunable diameter and spacing of double Ge quantum dots using highly-controllable spacers and selective oxidation of SiGe. *Sci Rep* **9**, 11303.
17. Chu CL, Luo GL, Chen LS, Chang WY, Wu WF, Yeh WK (2021) The first Ge nanosheets GAAFET CMOS inverters fabricated by 2D Ge/Si multilayer epitaxy, Ge/Si selective etching. In: *International Symposium on VLSI Technology, Systems and Applications (VLSI-TSA), Hsinchu, Taiwan*, pp 1–2.
18. Smagina ZV, Zinovyev VA, Zinovieva AF, Stepihova MV, Peretokin AV, Rodyakina EE, Dyakov SA, Novikov AV, et al (2022) Luminescent properties of spatially ordered Ge/Si quantum dots epitaxially grown on a pit-patterned “silicon-on-insulator” substrate. *J Lumin* **249**, 119033.
19. Peng Y, Miao L, Liu CY, Song HL, Kurosawa M, Nakatsuka O, Back SY, Rhyee JS, et al (2022) Constructed Ge quantum dots and Sn precipitate SiGeSn hybrid film with high thermoelectric performance at low temperature region. *Adv Energy Mater* **12**, 2103191.
20. Storozhevskiy MS, Arapkina LV, Novikov SM, Volkov VS, Arsenin AV, Uvarov OV, Yuryev VA (2022) Peculiarities and evolution of Raman spectra of multilayer Ge/Si (001) heterostructures containing arrays of low-temperature MBE-grown Ge quantum dots of different size and number density: Experimental studies and nu-

- merical simulations. *J Raman Spectrosc* **53**, 853–862.
21. Tripathi S, Sharma A, Shripathi T (2009) XPS study of annealing induced effects on surface and interface electronic properties of Si/Ge nanostructures. *Appl Surf Sci* **256**, 489–494.
  22. Shu Q, Huang P, Zhang X, Yang L, Ye D, Yang L, Liu H, Chen L (2023) Morphology and structure evolution of multilayered Ge/Si quantum dots grown by magnetron sputtering. *Micro Nano Lett* **18**, e12158.
  23. Rahim AFA, Hashim MR, Ali NK, Rusop M, Ooi J, Yusoff MZM (2013) Self-assembled Ge islands and nanocrystals by RF magnetron sputtering and rapid thermal processing: The role of annealing temperature. *Appl Surf Sci* **275**, 193–200.
  24. Samavati A, Mustafa MK, Othaman Z, Ghoshal SK (2015) Ge nanoislands grown by radio frequency magnetron sputtering: comprehensive investigation of surface morphology and optical properties. *J Nanomater* **2015**, 101–109.
  25. Shu Q, Wang R, Yang J, Zhang M, Zeng T, Sun T, Wang C, Yang Y (2018) Microstructure and optical response optimization of Ge/Si quantum dots transformed from the sputtering-grown Ge thin film by manipulating the thermal annealing. *Nanotechnology* **9**, 095601.
  26. Shu Q, Yang J, Chi Q, Sun T, Wang C, Yang Y (2018) Structure and optical properties of Ge/Si quantum dots formed by driving the evolution of Ge thin films via thermal annealing. *Jpn J Appl Phys* **4**, 045602.
  27. Ishikawa Y, Wada K, Liu JF, Cannon DD, Luan HC, Michel J, Kimerling LC (2005) Strain-induced enhancement of near-infrared absorption in Ge epitaxial layers grown on Si substrate. *J Appl Phys* **98**, 504–511.
  28. Floro JA, Sinclair MB, Chason E, Freund LB, Twisten RD, Hwang RQ, Lucadamo GA (2000) Novel SiGe island coarsening kinetics: Ostwald ripening and elastic interactions. *Phys Rev Lett* **84**, 701.
  29. Medeiros-Ribeiro G, Bratkovski AM, Kamins TI, Ohlberg DAA, Williams RS (1998) Shape transition of germanium nanocrystals on a silicon (001) surface from pyramids to domes. *Science* **279**, 353–355.
  30. Ross FM, Tromp RM, Reuter MC (1999) Transition states between pyramids and domes during Ge/Si island growth. *Science* **286**, 1931–1941.
  31. Kucherenko IV, Vinogradov VS, Melnik NN, Arapkina IV, Chapnin VA, Chizh KV, Yuryev VA (2008) The role of interdiffusion and spatial confinement in the formation of resonant Raman spectra of Ge/Si(100) heterostructures with quantum-dot arrays. *Phys Solid State* **50**, 1970–1977.
  32. Groiss H, Spindlberger L, Oberhumer P, Schäffler F, Fromherz T, Grydlik M, Brehm M (2017) Photoluminescence enhancement through vertical stacking of defect-engineered Ge on Si quantum dots. *Semicond Sci Technol* **32**, 02LT01.
  33. Zinovieva AF, Zinovyev VA, Nenashev AV, Teys SA, Dvurechenskii AV, Borodavchenko OM, Zhivulko VD, Mudryi AV (2020) Photoluminescence of compact GeSi quantum dot groups with increased probability of finding an electron in Ge. *Sci Rep* **10**, 9308.
  34. Vatankhah C, Ebadi A (2013) Quantum size effects on effective mass and band gap of semiconductor quantum dots. *Res J Recent Sci* **2**, 21–24.
  35. Chen PS, Pei Z, Peng YH, Lee SW, Tsai MJ (2004). Boron mediation on the growth of Ge quantum dots on Si (100) by ultrahigh vacuum chemical vapor deposition system. *Mater Sci Eng B ADV* **3**, 213–218.
  36. Wang KF, Zhang Y, Zhang W (2012). Morphology and photoluminescence of ultrasmall size of Ge quantum dots directly grown on Si (001) substrate. *Appl Surf Sci* **258**, 1935–1939.
  37. Shu QJ, Huang PR, Yang FH, Yang LJ, Chen L (2023) Study on crystal growth of Ge/Si quantum dots at different Ge deposition by using magnetron sputtering technique. *Sci Rep* **13**, 7511.